American Journal of Remote Sensing
2026, Vol. 14, No. 2, pp. 118–133
https://doi.org/10.11648/j.ajrs.20261402.17

Research Article

Rainfall–Surface Temperature Coupling and Compound Dry-Hot Persistence Across Northwestern Bangladesh: A 25-Year Multi-Sensor Earth Observation Analysis

Nafia Muntakim[1], Md. Imran Hossain[1], Zihad Ahmed[2], Md. Mizanoor Rahman[2,*]

[1]Institute of Environmental Science, University of Rajshahi, Rajshahi, Bangladesh

[2]Department of Geography and Environmental Studies, University of Rajshahi, Rajshahi, Bangladesh

Abstract

Understanding how rainfall variability regulates land-surface thermal conditions is essential for climate-sensitive regions where water availability, vegetation dynamics, and heat stress interact. However, the temporal persistence and spatial heterogeneity of rainfall–surface temperature relationships remain insufficiently characterized in northwestern Bangladesh. This study integrates 25 years (2001–2025) of multi-source Earth observation data, including Terra MODIS land-surface temperature (MOD11A2), MODIS vegetation index (MOD13A2), and CHIRPS precipitation, to quantify pre-monsoon hydrothermal coupling across 16 districts of the Rajshahi and Rangpur divisions. A total of 275 quality-controlled 8-day March–May composites were analyzed using Mann–Kendall trend tests, Sen's slope estimation, fixed-effects distributed lag models, and a locally standardized compound dry-hot persistence indicator. Mean daytime land-surface temperature ranged from 27.93°C in Kurigram to 31.38°C in Chapai Nawabganj. No district exhibited a significant daytime land-surface temperature trend after false-discovery-rate correction, whereas NDVI increased significantly across all districts. The distributed-lag model showed that 10 mm of concurrent rainfall was associated with a 0.164°C lower daytime land-surface temperature (95% CI: −0.224 to −0.103°C), while rainfall during the preceding 8–16 days was associated with a weaker effect (−0.093°C per 10 mm). The 16–24-day rainfall effect was not significant. Rainfall sensitivity varied considerably among districts, ranging from −0.538°C per 10 mm in Rajshahi to −0.123°C per 10 mm in Lalmonirhat. These findings demonstrate that satellite-derived hydrothermal responses are spatially heterogeneous and highlight the value of multi-sensor Earth observation frameworks for identifying location-specific climate adaptation priorities.

Keywords

Land-Surface Temperature, Precipitation, Distributed-Lag Model, NDVI, MODIS, CHIRPS, Bangladesh, Compound Dry-Hot Events

*Correspondence: Md. Mizanoor Rahman (mizangeo@ru.ac.bd)

Received: 31 August 2026; **Accepted:** 10 September 2026; **Published:** 28 September 2026

1. Introduction

Land surface temperature (LST) derived from satellite observations is a fundamental Earth observation variable for understanding surface energy exchange, evapotranspiration dynamics, and land–atmosphere interactions. Unlike near-surface air temperature measured at meteorological stations, LST provides spatially continuous information that captures thermal variability across heterogeneous landscapes, including croplands, urban areas, bare surfaces, and water bodies [1]. This capability has made satellite-based LST increasingly important for investigating regional-scale climate variability, ecosystem responses, drought impacts, and thermal stress patterns, particularly in regions with limited ground observations [2, 3]. Rainfall is a major hydroclimatic factor that regulates surface thermal conditions. Precipitation influences LST through multiple interacting mechanisms, including the reduction of incoming solar radiation by cloud cover, increased soil moisture availability, enhanced evaporative cooling, and vegetation-mediated transpiration [4-6]. However, the magnitude and duration of rainfall-associated thermal responses are not spatially uniform because they depend on the background climate, soil characteristics, vegetation conditions, land-cover composition, irrigation practices, and surface-water availability [7-9]. Therefore, understanding rainfall–LST interactions requires approaches that account for both temporal persistence and spatial heterogeneity rather than relying solely on seasonal averages or long-term temperature trends.

The northwestern region of Bangladesh is characterized by drought-prone and thermally stressed landscapes. The Barind Tract and adjacent alluvial plains depend on seasonal rainfall and irrigation. From March to May, high solar radiation occurs alongside an irregular transition to monsoonal moisture. Rainfall can alter the daytime LST through several linked pathways. Clouds reduce incoming shortwave radiation, wet soils increase the energy used for evaporation, and vegetation can sustain evapotranspiration after a rain event [5, 6, 10]. At an 8-day temporal resolution, the concurrent association encompasses cloud-radiative, wet-surface, and moisture-recycling pathways, whereas a subsequent composite association may reflect residual surface and root zone moisture [11]. Previous remote sensing studies have documented changes in land cover, urban heat islands, and rising surface temperatures in specific northwestern settlements [12]. Studies integrating satellite-derived LST, vegetation indices, and climate variables have improved our understanding of the thermal dynamics and feedback loops among precipitation, vegetation, and temperature [13]. Moderate Resolution Imaging Spectroradiometer (MODIS) LST products are particularly valuable because of their extensive temporal coverage [14], whereas MODIS vegetation indices provide insights into vegetation and energy regulation [15]. A given amount of rainfall may not produce the same thermal response. Local factors, such as soil characteristics, water retention, vegetation density, urban cover, and river influences, can affect sensitivity. There are strong correlations between vegetation abundance and LST because vegetation mediates heat fluxes [16]. Recent studies have linked heat, drought, vegetation stress, and groundwater pressure in the Barind Tract [8, 17-19]. However, many studies have focused more on spatial patterns and warming trends than on quantifying the response of surface temperature to rainfall variability [20-22].

Regional trend evidence also cautions against treating the thermal landscape as a single, monotonic signal. MODIS analyses have found spatially mixed warming and cooling across South Asia, with vegetation and irrigated agriculture among the proposed influences [23-25]. Studies in western Bangladesh have reported precipitation and surface water as thermal moderators [26-28], whereas a national analysis has identified important day–night and climate interactions [29]. Together, this literature suggests that trend direction alone provides an incomplete account of thermal risk. A process-oriented analysis should combine a long-term spatial context with short-term hydroclimatic controls that produce hot or cool surface states [30]. This study, therefore, posed four questions: (1) How are March–May daytime LST, rainfall, and vegetation distributed across the 16 districts of the Rajshahi and Rangpur divisions? (2) Did the district-scale pre-monsoon LST, rainfall, or NDVI change monotonically from 2001 to 2025? (3) How strongly is daytime LST associated with concurrent and antecedent rainfall after controlling for district, seasonal position, year, and NDVI? (4) How much does the concurrent rainfall–LST association vary among districts? This study aims to develop a framework for analyzing pre-monsoon hydrothermal coupling across districts by using long-term satellite observations and statistical modeling. The findings go beyond urban heat island assessments, enhancing our understanding of hydrothermal dynamics in climate-sensitive areas and supporting tailored land and water management strategies.

2. Materials and Methods

2.1. Study Area

The study area comprises all 16 districts in the Rajshahi and Rangpur divisions of northwestern Bangladesh, covering approximately 34,472km^2 (Figure 1). Rajshahi Division includes Bogura, Joypurhat, Naogaon, Natore, Chapai Nawabganj, Pabna, Rajshahi, and Sirajganj; Rangpur Division includes Dinajpur, Gaibandha, Kurigram, Lalmonirhat, Nilphamari, Panchagarh, Rangpur, and Thakurgaon. For reproducibility, the source administrative attributes retain the Food and Agriculture Organization Global Administrative Unit Layers (GAUL) spellings “Bogra” and “Nawabganj,” whereas the manuscript uses the current display names Bogura and Chapai

Nawabganj. The region spans the relatively dry western Barind landscape, intensively cultivated plains, and wetter northern and eastern riverine districts of Bangladesh [31, 32]. March–May (MAM) was selected because it captures the season of the greatest pre-monsoon surface heating and the onset of convective rainfall.

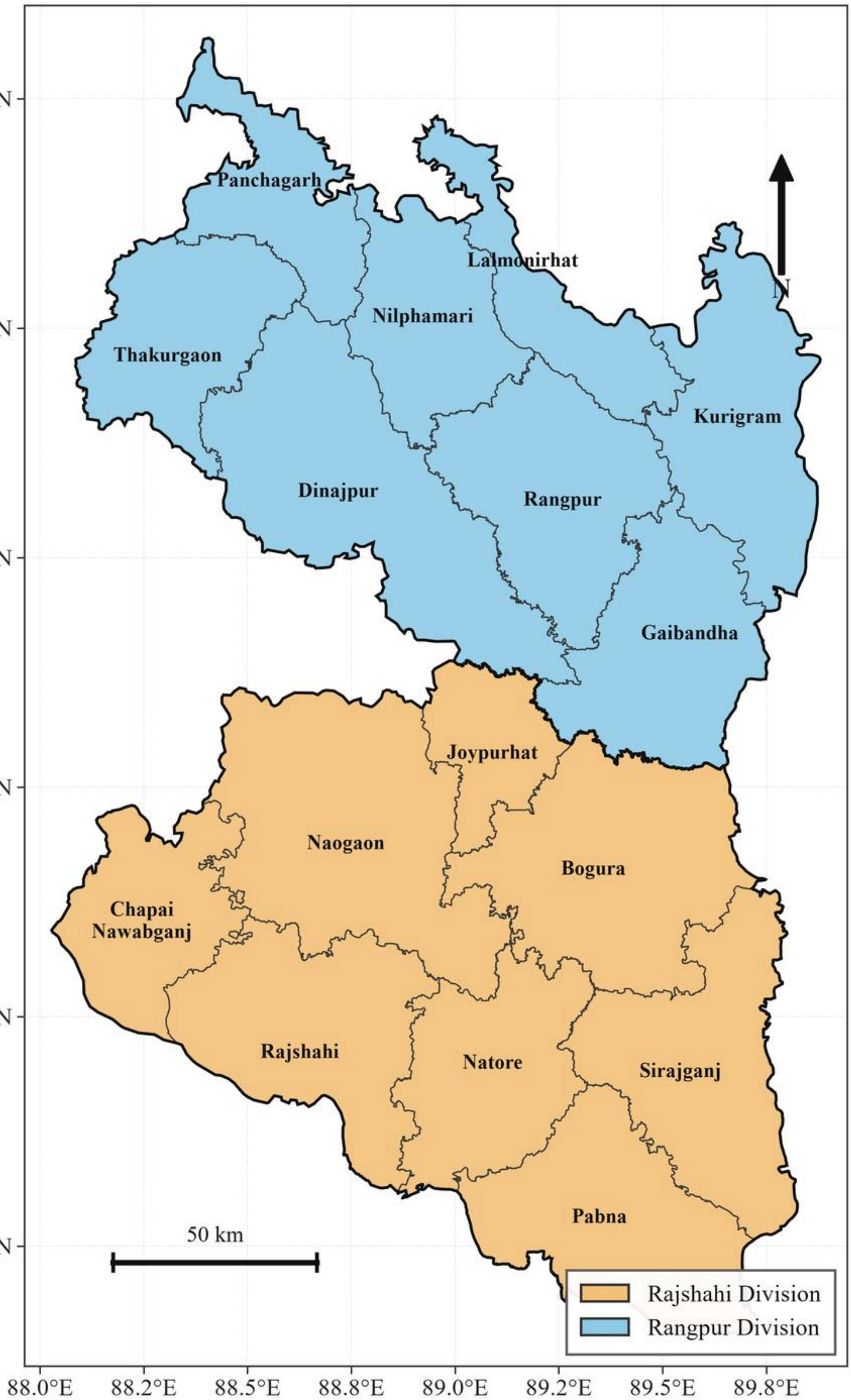

Figure 1. Location of the 16 study districts in the Rajshahi and Rangpur divisions of northwestern Bangladesh. District polygons follow FAO GAUL 2015 level-2 boundaries; current display names are used where they differ from source attributes.

2.2. Earth Observation and Climate Datasets

A multi-source Earth observation framework was developed by integrating satellite-derived land-surface temperature, vegetation conditions, precipitation observations, and administrative boundaries. All datasets were processed using reproducible JavaScript-based workflows within Google Earth Engine [33]. The analysis covered the period from 1 January 2001 to 31 December 2025. The study period was selected because Terra MODIS provides consistent long-term LST observations beginning in 2000, and to exclude 2000 to avoid incomplete annual coverage. Analysis was restricted to MODIS composites from March to May, yielding 275 potential 8-day observation periods over 25 years. The datasets used in this study are summarized in Table 1.

Table 1. Datasets used in the analysis.

Variable	Dataset	Resolution	Bands/use	Citation
Land-surface temperature	Terra MODIS MOD11A2 v6.1	1 km; 8 days	LST_Day_1km, LST_Night_1km and QA	[14]
Vegetation	Terra MODIS MOD13A2 v6.1	1 km; 16 days	NDVI and SummaryQA	[34]
Rainfall	CHIRPS Daily	0.05°; daily	Precipitation totals	[35]
Administrative boundaries	FAO GAUL 2015 level 2	District polygons	16 districts in two divisions	[36]

2.3. Quality Control and Temporal Alignment

MOD11A2 daytime and nighttime LST values were converted from the native scaled integer format to degrees Celsius using the product scale factor (0.02), followed by the subtraction of 273.15. Quality filtering was performed using MODIS quality assurance (QA) information. Pixels were retained only when mandatory quality indicators identified valid observations, data-quality conditions were acceptable, and the reported LST error was ≤ 2 K. No additional emissivity correction was applied because MOD11A2 is an operational, validated LST product whose Collection 6 retrievals have been assessed against in situ measurements and shown to be reliable for detecting temporal variability [14, 37-39]. MOD13A2 normalized difference vegetation index (NDVI) values were converted using a product scale factor of 0.0001. Pixels with good or marginal Summary QA conditions were retained. These procedures ensured consistent, quality-controlled estimates of surface temperature and vegetation conditions throughout the study period.

To investigate the effects of rainfall timing, each MODIS 8-day LST composite was temporally aligned with three non-overlapping Climate Hazards Group Infrared Precipitation with Stations (CHIRPS) rainfall periods [40]:

1) Concurrent rainfall (0–8 days): precipitation accumulated during the same composite period.
2) Lag-1 rainfall (8–16 days): precipitation accumulated during the immediately preceding 8-day period.
3) Lag-2 rainfall (16–24 days): precipitation accumulated during the preceding 16–24-day period.

A cumulative 24-day rainfall variable was also generated for climatological analysis. NDVI values were represented by the mean observations within ±8 days of each LST acquisition date to match the thermal observation period. Each aligned observation was aggregated from pixels to district-level averages, producing a potential dataset of 4,400 district–date observations (275 composites × 16 districts). For daytime LST modelling, observations were retained if at least 50% of district pixels had valid MODIS observations. Additional sensitivity analyses were conducted using 40% and 60% valid-pixel thresholds to evaluate the influence of spatial data availability.

2.4. Spatial Analysis, Trend Assessment, and Compound Dry-Hot Persistence

Five-year MAM climatologies (2001–2005, 2006–2010, 2011–2015, 2016–2020, and 2021–2025) were mapped using consistent visualization scales to allow for comparison among periods. Early-to-recent changes were calculated as the difference between the 2021–2025 and 2001–2005 means. Long-term pixel-level LST trends were estimated using Sen's slope estimator [41], given in Equation (1).

$$\hat{\beta} = \text{median}\left(\frac{x_j - x_i}{t_j - t_i}\right), 1 \leq i < j \leq n \tag{1}$$

That is, the slope estimate β̂ is the median of all pairwise slopes (x_j − x_i)/(t_j − t_i), where x_i and x_j are the values of the variable in years t_i and t_j respectively, taken over every pair 1 ≤ i < j ≤ n, and n is the number of years in the record.

At the district level, the annual mean values of LST, NDVI, and rainfall for March–May were evaluated using the Mann–Kendall non-parametric trend test [42]. Sen's median slope was used to estimate the magnitude of the trend. Because multiple districts and variables were tested simultaneously, the Benjamini–Hochberg false discovery rate (FDR) correction was applied separately to each trend family [43]. Statistical significance was defined as FDR-adjusted $p < 0.05$.

Compound dry-hot persistence was defined at each pixel as the percentage of valid 8-day MAM composites in which daytime LST exceeded the local 90th percentile and concurrent rainfall was below the local 20th percentile. We define these thresholds for this study; they are not taken from a published index. This indicator measures unusual co-occurrence and persistence relative to each pixel's own history rather than absolute heat or drought severity. Because the percentiles are local, a pixel's persistence value is expressed relative to its own climatological distribution and is therefore comparable across the regional gradient as a measure of relative anomaly, but it is not comparable between pixels as a measure of absolute heat severity. Because the metric uses satellite LST and an 8-day rainfall total, it must not be interpreted as a meteorological heatwave or a direct measure of human heat exposure. This percentile-based definition follows the logic of compound event analysis while adapting it to local surface climatology [44, 45].

2.5. Distributed-Lag Modeling and District-Level Sensitivity Analysis

The primary inferential model regressed district-mean daytime LST on concurrent rainfall, two antecedent rainfall windows, and NDVI. The rainfall coefficients were expressed per 10 mm and NDVI per 0.1 unit. Fixed effects for the district absorbed time-invariant spatial differences; day-of-year fixed effects controlled the repeating pre-monsoon seasonal cycle; and year fixed effects absorbed region-wide interannual shocks. Because observations shared both district and composite dates, uncertainty was estimated using two-way cluster-robust covariance for district and observation date. Small-cluster t-inference was applied to the 16 district clusters. Additional robustness analyses include district-clustered covariance and Driscoll–Kraay covariance estimators with lag-2 correction. The model estimates were interpreted as conditional associations rather than as causal effects. Although fixed effects and robustness tests reduce several sources of bias, the observational design cannot fully isolate rainfall-driven thermal responses from unmeasured processes, such as irrigation, soil moisture variation, cloud conditions, and land cover changes [46-48].

To examine spatial heterogeneity, we estimated separate district-level models for concurrent rainfall sensitivity. These models controlled for rainfall lags, NDVI, seasonal position, and yearly effects. Heteroskedasticity-and-autocorrelation-consistent (HAC) standard errors with two 8-day lags were applied, and district-level significance values were adjusted using the FDR procedure. Nighttime LST and day–night temperature range models were evaluated only as exploratory analyses because nighttime clear-sky MODIS coverage was insufficient for reliable district-scale inference [49, 50].

3. Results

3.1. Data Coverage and the Regional Thermal–Hydroclimatic Gradient

The multi-source Earth observation framework generated 4,400 potential district–composite observations from 275 March–May MODIS LST periods across 16 districts during 2001–2025. The availability and quality of daytime and nighttime MODIS observations after quality filtering are summarized in Table S1. Daytime observations showed consistently high spatial coverage, with a mean valid-pixel coverage of 92.43% across all district–date combinations. After applying the primary 50% valid-pixel threshold, 4,130 observations (93.86%) were retained for daytime statistical modelling. The retained observations were comparable across alternative thresholds, with 4,187 at the 40% threshold and 4,068 at the 60% threshold. In contrast, nighttime MODIS observations showed substantially lower availability. Mean nighttime valid-pixel coverage was only 9.89%, and only 93 observations (2.11%) met the 50% threshold requirement. Therefore, all primary analyses were conducted using daytime LST, while nighttime results were evaluated only as exploratory sensitivity analyses. The long-term March–May hydrothermal characteristics across the study region are presented in Table 2 and Figure 2.

District-level daytime LST showed a clear spatial gradient, with mean values ranging from 27.93°C in Kurigram to 31.38°C in Chapai Nawabganj. The warmest conditions occurred mainly in southwestern districts, including Chapai Nawabganj (31.38°C), Pabna (31.24°C), and Rajshahi (31.12°C), whereas northern districts such as Kurigram (27.93°C), Nilphamari (27.94°C), and Rangpur (28.14°C) exhibited comparatively lower surface temperatures. This thermal pattern corresponded with spatial differences in rainfall and vegetation conditions. Mean concurrent 8-day rainfall was highest in Kurigram (54.51 mm) and lowest in Chapai Nawabganj (19.10 mm) and Rajshahi (19.68 mm). The correspondence between rainfall and vegetation condition was broad but not monotonic. NDVI was generally higher in the wetter northern districts and lower in the comparatively drier western districts, but two northern districts departed from this pattern: Kurigram combined the highest mean concurrent rainfall in the study region (54.51 mm) with the lowest district-mean NDVI (0.475), and Gaibandha likewise paired high rainfall (41.80 mm) with a comparatively low NDVI (0.532) (Table 2; Figure 2). District-mean NDVI therefore reflects surface composition as well as water availability, and should not be read as a direct index of moisture supply. The resulting spatial pattern indicates a distinct dry-hot southwestern zone and a cooler, wetter northern and northeastern zone across northwestern Bangladesh.

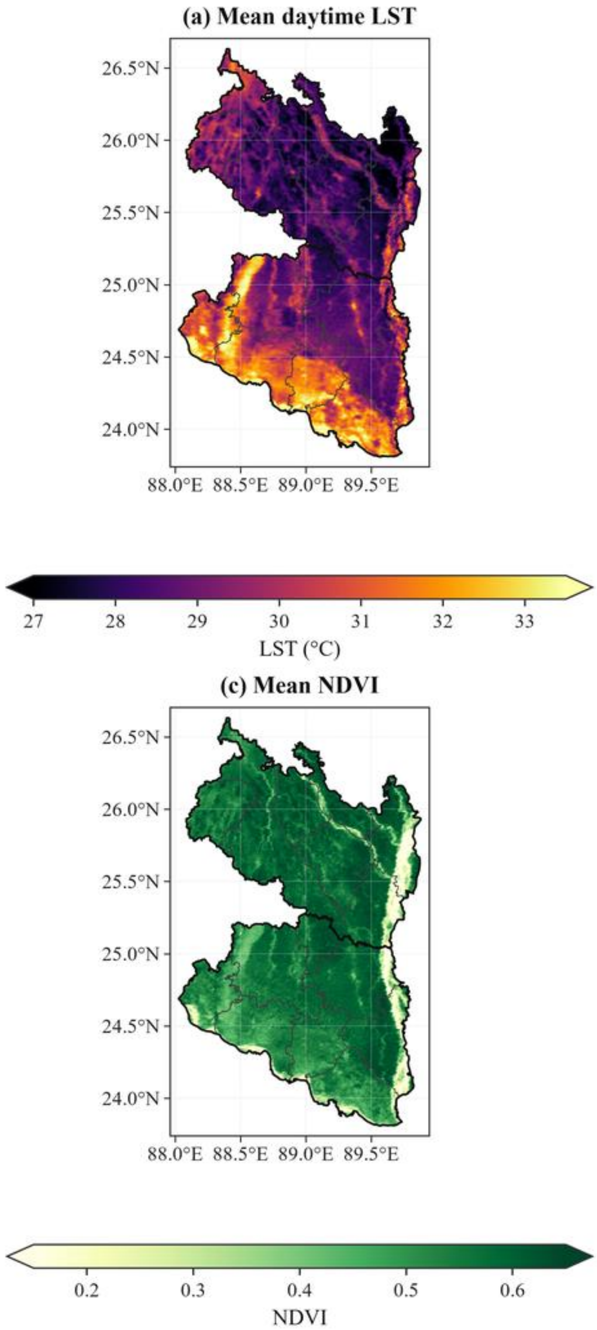

Figure 2. *Long-term March–May hydroclimatic context, 2001–2025. (a) Mean daytime land-surface temperature; (b) mean nighttime land-surface temperature; (c) mean normalized difference vegetation index; (d) mean March–May rainfall total. Common district boundaries permit direct comparison of the dry-hot southwest with wetter and generally cooler northern and eastern districts. Panel (d) shows seasonal March–May totals and is therefore on a different scale from the 8-day and 24-day rainfall windows reported in Table 2. Data: MODIS MOD11A2 LST, MODIS MOD13A2 NDVI and CHIRPS Daily rainfall.*

Table 2. *District-level March–May climatology (2001–2025). Nighttime statistics are excluded from the main table because of sparse valid coverage.*

Division	District	Day LST (°C)	NDVI	Rain 0–8 d (mm)	Rain 0–24 d (mm)
Rajshahi	Bogura	28.67	0.555	30.62	72.67
Rajshahi	Joypurhat	28.46	0.598	30.95	74.01
Rajshahi	Naogaon	29.64	0.544	22.46	54.43
Rajshahi	Natore	30.97	0.524	27.21	65.68
Rajshahi	Chapai Nawabganj	31.38	0.481	19.10	45.44
Rajshahi	Pabna	31.24	0.483	28.90	70.69
Rajshahi	Rajshahi	31.12	0.488	19.68	47.57
Rajshahi	Sirajganj	29.10	0.505	33.40	80.71
Rangpur	Dinajpur	28.29	0.585	30.69	71.99
Rangpur	Gaibandha	28.40	0.532	41.80	99.53
Rangpur	Kurigram	27.93	0.475	54.51	130.85
Rangpur	Lalmonirhat	28.25	0.578	46.88	110.99
Rangpur	Nilphamari	27.94	0.591	38.07	88.66
Rangpur	Panchagarh	29.35	0.560	36.33	85.36
Rangpur	Rangpur	28.14	0.582	40.18	95.94
Rangpur	Thakurgaon	29.21	0.562	31.25	72.61

3.2. Multi-Temporal Evolution of Daytime LST, Rainfall, and Vegetation

The five-year climatological evolution of daytime LST during 2001–2025 is illustrated in Figure 3. The results show substantial inter-period variability superimposed on a persistent spatial thermal gradient. The regional mean daytime LST increased from 29.28°C during 2001–2005 to 29.84°C during 2006–2010, declined to 28.89°C during 2016–2020, and reached 29.37°C during 2021–2025. The difference between the earliest and latest periods was therefore relatively small, with a regional mean change of +0.09°C. Pixel-level Sen slope analysis revealed spatially heterogeneous thermal trends rather than a consistent regional warming pattern (Figure 3). The median pixel-level daytime LST slope was −0.009°C year^{-1}, with the 5th–95th percentile ranging from −0.104 to +0.059°C year^{-1}. Both increasing and decreasing thermal tendencies were distributed across the study region.

District-scale Mann–Kendall trend results for daytime LST, NDVI, and rainfall are provided in Table S3. After FDR correction, none of the 16 districts exhibited a significant daytime LST trend. Chapai Nawabganj showed the strongest apparent cooling tendency (Sen slope = −0.066°C year^{-1}; unadjusted $p = 0.006$), although this relationship was not significant after multiple-testing correction (FDR-adjusted $p = 0.101$). Similarly, no district showed a significant March–May rainfall trend after FDR adjustment (Table S3). In contrast, NDVI exhibited significant positive trends across all districts, with Sen slopes ranging from +0.0032 year^{-1} in Gaibandha to +0.0095 year^{-1} in Panchagarh. These results indicate widespread vegetation greening during the study period, while daytime LST trends remained spatially variable and statistically nonsignificant at the district scale.

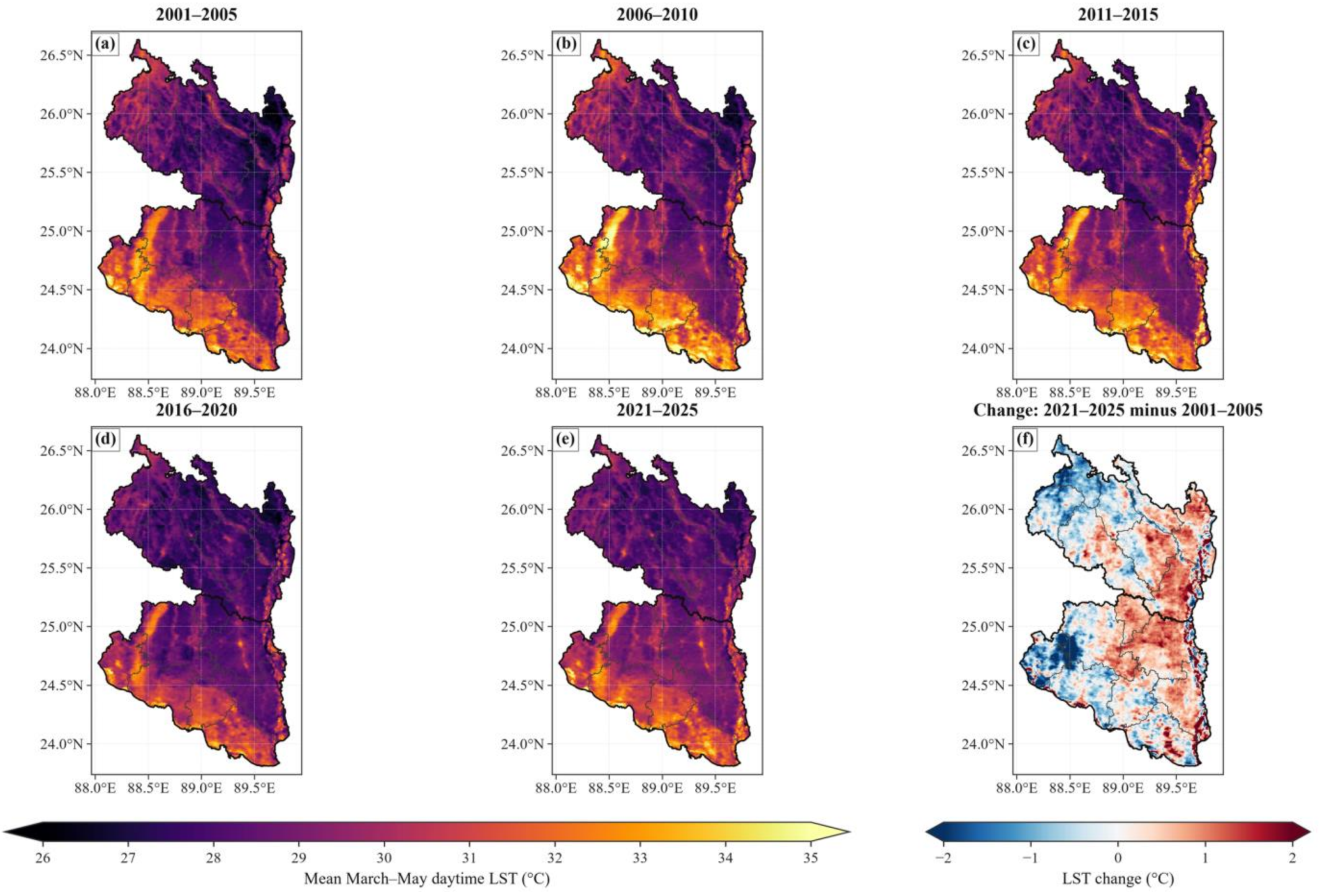

Figure 3. *Five-year March–May daytime land-surface temperature climatologies and early-to-recent change. Change is the 2021–2025 mean minus the 2001–2005 mean. All panels are clipped to the exact study boundary.*

3.3. Temporal Characteristics of Rainfall–Surface Temperature Coupling

The fixed-effects distributed-lag model results are summarized in Table 3, while the temporal rainfall response patterns and district-level sensitivity estimates are illustrated in Figure 4. The pooled fixed-effects model explained 53.7% of the variance in daytime LST (adjusted $R^2 = 0.531$; n = 4,130). Each additional 10 mm of concurrent rainfall was associated with 0.164°C lower daytime LST (two-way-clustered 95% CI: −0.224 to −0.103; $p < 0.001$). Rainfall during the preceding 8–16 days retained a smaller association of −0.093°C per 10 mm (95% CI: −0.157 to −0.028; p = 0.008). The 16–24-day lag was close to zero and nonsignificant (−0.007°C; 95% CI: −0.073 to +0.058; p = 0.816). The sequence indicates a strong same-composite association, a residual association in the next 8-day period, and little detectable association thereafter.

Vegetation remained independently associated with cooler surfaces after rainfall and the inclusion of fixed effects. A 0.1 increase in NDVI was associated with 0.786°C lower daytime LST (95% CI: −1.108 to −0.465; $p < 0.001$). This magnitude should be interpreted as an adjusted association, not as the temperature effect of an intervention, because NDVI may also capture irrigation, crop calendar, soil moisture, and unmeasured land-cover differences. The concurrent and lag-1 estimates were nearly unchanged at the 40%, 50%, and 60% valid-pixel thresholds (concurrent: −0.161 to −0.165°C per 10 mm; lag 1: −0.092 to −0.095°C per 10 mm) and remained significant under district-clustered and Driscoll–Kraay inference (Table S4).

Table 3. *Distributed-lag fixed-effects model for daytime LST. Coefficients were adjusted for district, day of year, and year; confidence intervals use two-way clustering by district and composite date with small-cluster t inference (n = 4,130; $R^2 = 0.537$; adjusted $R^2 = 0.531$).*

Predictor	Estimate (°C)	95% CI	p value
Rainfall, concurrent (0–8 d), per 10 mm	−0.164	−0.224, −0.103	<0.001

Predictor	Estimate (°C)	95% CI	p value
Rainfall, lag 1 (8–16 d), per 10 mm	−0.093	−0.157, −0.028	0.008
Rainfall, lag 2 (16–24 d), per 10 mm	−0.007	−0.073, +0.058	0.816
NDVI, per 0.1	−0.786	−1.108, −0.465	<0.001

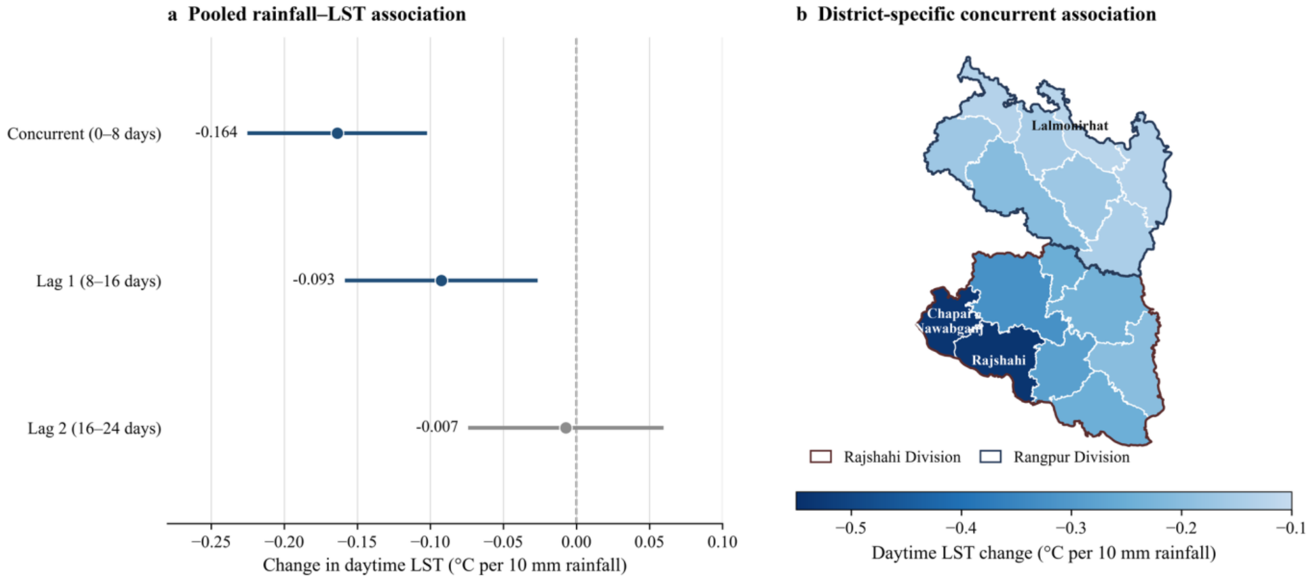

Figure 4*. Rainfall-linked daytime surface cooling. (a) Pooled distributed-lag coefficients with two-way-clustered 95% confidence intervals. (b) District-specific concurrent rainfall sensitivity after adjustment for both rainfall lags, NDVI, seasonal position, and year. Darker blue indicates a larger negative LST association per 10 mm rainfall. District, day-of-year and year fixed effects; 95% confidence intervals clustered by district and composite date (n = 4,130).*

3.4. Spatial Heterogeneity of Rainfall Sensitivity and Compound Dry-Hot Persistence

District-specific rainfall sensitivity estimates are presented in Table S2 and mapped in Figure 4. Concurrent cooling sensitivity was negative across all districts and remained significant after FDR correction. Using two-lag heteroskedasticity-and-autocorrelation-consistent intervals, the strongest rainfall-associated temperature responses occurred in Rajshahi and Chapai Nawabganj. In Rajshahi, a 10 mm increase in concurrent rainfall was associated with a 0.538°C decrease in daytime LST (95% CI: −0.692 to −0.384), while Chapai Nawabganj showed a similar response of 0.537°C decrease per 10 mm rainfall (95% CI: −0.710 to −0.363). In contrast, Lalmonirhat showed the weakest response, with a 0.123°C decrease per 10 mm rainfall (95% CI: −0.185 to −0.060). The difference between the strongest and weakest district responses was approximately 4.4-fold (Table S2; Figure 4).

Across the study region, compound dry-hot conditions occurred in an average of 1.75% of valid March–May composites. The 95th percentile of persistence was 5.04%, with localized maximum values reaching 7.75%. The spatial pattern of compound dry-hot persistence did not match rainfall sensitivity. Areas with frequent dry-hot surface conditions and areas with stronger rainfall-associated temperature responses represented different aspects of hydrothermal vulnerability. Therefore, these indicators provide complementary information rather than a single measure of climate risk (Figure 5).

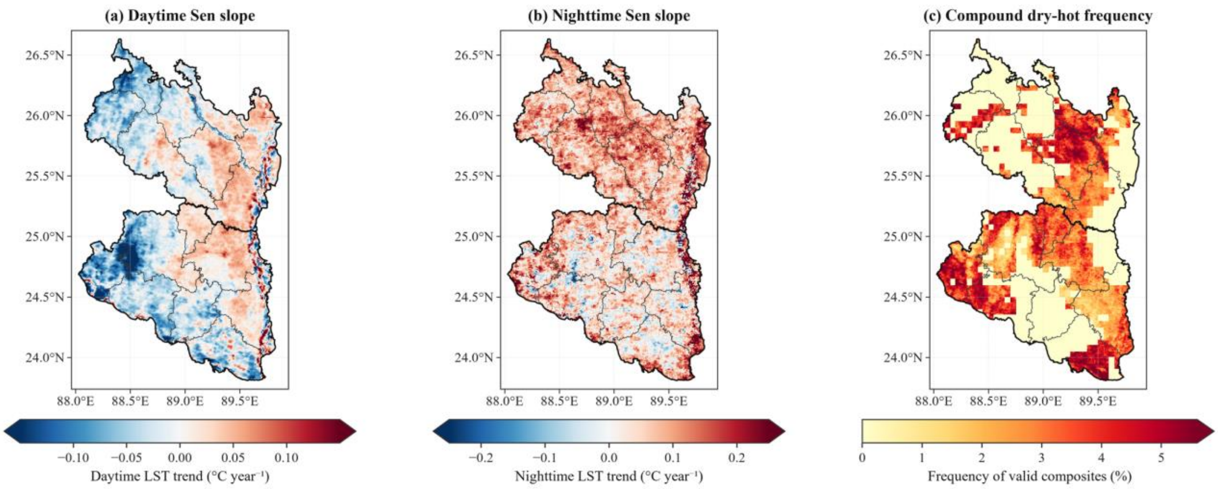

Figure 5. *Pixel-wise March–May Sen slopes and compound dry-hot persistence, 2001–2025. (a) Daytime LST Sen slope; (b) nighttime LST Sen slope; (c) compound dry-hot frequency. Persistence is the percentage of valid 8-day composites with local daytime LST above the 90th percentile and concurrent rainfall below the 20th percentile; it is a land-surface condition, not a meteorological heatwave definition. Nighttime interpretation in panel (b) is limited by sparse clear-sky coverage.*

3.5. Nighttime Observations: Coverage Limits and Exploratory Results

Exploratory nighttime analyses were conducted to evaluate whether similar rainfall–temperature relationships could be detected under nighttime MODIS observations. The limitations of nighttime data coverage are shown in Table S1 and Figure S2. Due to sparse clear-sky nighttime observations, only 93 district–date observations satisfied the primary 50% coverage threshold (Table S1). The nighttime distributed lag model did not identify significant associations among rainfall, NDVI, and nighttime LST. Similarly, the day–night temperature range model retained only 80 observations and produced unstable uncertainty estimates. Therefore, these analyses were not used for regional inference. The absence of significant nighttime relationships should not be interpreted as evidence that rainfall and vegetation have no nocturnal thermal influence. Rather, the results demonstrate the limitation of clear-sky thermal infrared observations for nighttime regional-scale analysis (Table S1; Figure S2). Nighttime climatologies and trends are nevertheless shown alongside their daytime counterparts in Figures 2 and 5 so that the scale of the coverage limitation is visible to the reader rather than stated only in the text. Those panels describe data availability and are not used to support any inference in this paper.

4. Discussion

4.1. A Hydrothermal Landscape, not a Single Warming Surface

The results demonstrate that pre-monsoon thermal conditions across northwestern Bangladesh are shaped by the combined influences of rainfall availability, vegetation dynamics, and landscape characteristics rather than a single regional warming trajectory. The persistent thermal gradient, with warmer surfaces in the drier southwestern districts and cooler conditions in the wetter northern areas, reflects differences in surface energy partitioning. Districts such as Chapai Nawabganj, Pabna, and Rajshahi exhibited higher daytime LST with lower rainfall and NDVI, whereas northern districts such as Kurigram and Nilphamari showed comparatively cooler surface temperatures under wetter, more vegetated conditions. The absence of a significant district-scale daytime LST trend after FDR correction does not imply the absence of climate-related thermal changes. Instead, it highlights the importance of interpreting satellite-derived LST within its spatial and temporal contexts. Unlike air temperature, LST represents the radiometric temperature of the land surface at the time of satellite observation and is strongly influenced by vegetation cover, soil moisture, irrigation, land cover composition, and surface properties [1, 51]. Therefore, seasonal and landscape-scale LST trends may differ from broader atmospheric warming signals.

Previous remote sensing studies in Bangladesh have documented warming patterns associated with urban expansion, land cover transformation, and selected locations [52-54]. However, these localized signals may not reflect the broader regional landscape, in which croplands, river corridors, vegetation, and water bodies modify thermal responses. Consistent with South Asian evidence showing contrasting daytime and nighttime thermal trends across different landscapes [25], and recent findings that precipitation and surface water regulate LST variability in western Bangladesh [52, 55, 56], this study demonstrates that thermal change assessment requires consideration of hydroclimatic and landscape control. A city may experience thermal intensification while its surrounding district remains moderated by vegetation, moisture availability, and surface characteristics [57].

4.2. Rainfall–LST Coupling Is Concentrated in the Concurrent and Next Composite

The distributed-lag sequence provides the main process-level contribution to this study. The concurrent coefficient was the largest, the 8–16-day coefficient remained substantial, and the 16–24-day coefficient disappeared. This ordering is physically plausible because cloud cover and rainfall reduce the available surface energy during the composite, whereas evaporation from wet soil and transpiration can continue after rain. Increased soil moisture after rainfall can enhance latent heat flux and evaporative cooling, while soil moisture persistence can maintain delayed land–atmosphere responses beyond the precipitation event [58, 59]. As moisture is depleted, the marginal association decays. A previous study similarly emphasized that precipitation–surface temperature relationships contain a meaningful lag structure rather than a single contemporaneous correlation [13]. However, because the temporal unit is an 8-day composite, the analysis resolves short-lived coupling, not an instantaneous post-event temperature response.

The coefficients must be interpreted as conditional associations. Rainfall timing, cloudiness, and LST retrieval are linked because thermal-infrared observations require sufficiently clear conditions; the same-composite coefficient can therefore include cloud-radiative effects, clear-sky selection, wet-surface and evapotranspirative pathways [50, 60]. District, seasonal position, and year fixed effects reduce several confounding pathways, two-way clustering addresses common-date dependence, and the persistence of the lag-1 association after controlling for concurrent rainfall and NDVI is consistent with a residual hydrothermal response [58, 61]. However, this is not proof of the mechanism. The analysis does not directly observe soil moisture, irrigation withdrawals, crop type, or cloud optical properties, and causal attribution would require additional measurements or a quasi-experimental design.

4.3. Vegetation Greening May Buffer Daytime Heating

All districts showed significant positive NDVI trends, and NDVI was strongly and negatively associated with daytime LST in the multivariate model. Vegetation can cool the surface through shading and latent heat exchange, whereas irrigated crops can maintain transpiration during dry periods. This finding is consistent with the established inverse LST–vegetation relationship [16] and with broader MODIS evidence that natural vegetation and irrigated agriculture contribute to regional cooling [25]. The NDVI trend may partly explain why a uniform daytime warming signal did not emerge at the district scale despite intensifying heat concerns. Greening should not be automatically equated with ecological restoration. In northwestern Bangladesh, this may reflect crop intensification, irrigation, changes in seasonal planting, tree cover, or improved canopy conditions. Some forms of irrigated greening can cool the surface while increasing groundwater demand, which is a serious concern in the Barind region. Therefore, thermal adaptation should evaluate both cooling benefits and water costs.

4.4. Why District Sensitivity Matters for Adaptation

A more-than-fourfold sensitivity range is policy-relevant. In Rajshahi and Chapai Nawabganj, an increase in rainfall was associated with a much larger reduction in surface temperature than in Lalmonirhat and Kurigram. One plausible explanation is the diminishing marginal response: wetter northern districts already have greater background moisture, whereas dry western surfaces can shift sharply from sensible to latent heat flux when water becomes available [62]. Soil texture, vegetation structure, irrigation, and land cover may also contribute [63]. These mechanisms require direct testing, but the mapped heterogeneity already shows why a single northwest-wide coefficient is insufficient. The sensitivity and persistence maps can be used to screen districts for follow-up assessments of water retention, vegetation, and recurrent dry-hot surface conditions. Candidate measures include the protection of ponds, canals, and floodplain storage; improved soil moisture retention; shaded and vegetated corridors within settlements; and irrigation scheduling to reduce evaporative losses. The observational coefficients do not estimate the effect of any intervention; therefore, these options require local hydrological, agronomic, and equity assessments before implementation. In groundwater-stressed areas of the Barind Tract, water-intensive cooling strategies could transfer thermal risk into water-security risk.

4.5. Limitations and Future Research

First, MOD11A2 describes clear-sky land-surface skin temperature at the Terra overpass time, not daily maximum air temperature or human heat exposure. Second, MODIS 1-km pixels mix land-cover types and cannot resolve neighborhood-scale thermal features. Third, CHIRPS has a coarser native grid than MODIS and may smooth convective rainfall. Fourth, the district models do not include soil moisture, irrigation, groundwater depth, crop type, albedo or elevation. Fifth, thermal-infrared cloud screening creates nonrandom missingness, especially at night, and can also affect the interpretation of same-composite rainfall. Sixth, inference relies on only 16 district clusters; two-way clustering and sensitivity analyses strengthen but do not eliminate small-cluster concerns. District-specific coefficients should be interpreted as comparative estimates rather than immutable physical constants.

Future work should integrate soil-moisture products, irrigation calendars, land-cover fractions and groundwater observations; compare Terra with Aqua and geostationary temperature data; and validate satellite LST against station air temperature and field surface measurements. A multilevel model could estimate district variation with partial pooling, while event-based analysis could test whether cooling differs by rainfall intensity, antecedent dryness or crop stage. The nighttime question requires an all-weather or gap-filled temperature product rather than reliance on the sparse clear-sky district panel used here.

5. Conclusions

Across 16 districts and 25 pre-monsoon seasons, northwestern Bangladesh did not behave as one uniformly warming land surface. Its daytime thermal geography was characterized by a persistent dry-hot southwest, a cooler and wetter north and east, widespread NDVI greening, and spatially mixed local LST tendencies. The strongest statistical result was temporal: rainfall was associated with lower daytime LST in the same 8-day composite, a weaker residual association during the following composite, and no detectable association at 16–24 days. Vegetation was independently associated with lower daytime LST, and the rainfall estimates survived stricter two-way-clustered and threshold-sensitivity analyses.

The association was also geographically unequal. Rajshahi and Chapai Nawabganj showed sensitivities more than four times that of Lalmonirhat. This heterogeneity, together with localized compound dry-hot persistence, supports district-specific screening for land and water planning. Water-storage protection, vegetation maintenance, and soil-moisture retention are testable adaptation candidates, not effects established by this observational study, and they must be evaluated against groundwater constraints. Code-based integration of MODIS and CHIRPS can therefore move LST research beyond descriptive change maps toward a temporally explicit hydroclimate analysis while preserving the distinction between association, mechanism, and intervention.

Abbreviations

CHIRPS	Climate Hazards Group Infrared Precipitation with Stations
CI	Confidence Interval
FDR	False Discovery Rate
GAUL	Global Administrative Unit Layers
HAC	Heteroskedasticity-and-Autocorrelation-Consistent
LST	Land Surface Temperature
MAM	March–April–May
MODIS	Moderate Resolution Imaging Spectroradiometer
NDVI	Normalized Difference Vegetation Index
QA	Quality Assurance

Supplementary Material

The supplementary material can be accessed at https://doi.org/10.11648/j.ajrs.20261402.17

Author Contributions

Nafia Muntakim: Conceptualization, Formal Analysis, Methodology, Resources, Writing – original draft

Md. Imran Hossain: Software, Validation, Visualization

Zihad Ahmed: Data curation, Formal Analysis

Md. Mizanoor Rahman: Supervision, Writing – review & editing

Data Availability Statement

All primary datasets analysed in this study are publicly available. Terra MODIS land-surface temperature (MOD11A2 Version 6.1) and vegetation index (MOD13A2 Version 6.1) products are distributed by the NASA Land Processes Distributed Active Archive Center and are accessible through Google Earth Engine [14, 34]. CHIRPS Daily precipitation is distributed by the Climate Hazards Center and is likewise accessible through Google Earth Engine [35]. District boundaries follow the FAO Global Administrative Unit Layers 2015 level-2 dataset, available through the Earth Engine Data Catalog [36].

The Google Earth Engine processing script, the derived 8-day district panel, the statistical analysis scripts and the result tables generated during this study are available from the corresponding author upon reasonable request.

Conflicts of Interest

The authors declare no conflicts of interest.

References

[1] Li, Z., Wu, H., Duan, S., Zhao, W., Ren, H., Liu, X., Leng, P., Tang, R., Ye, X., Zhu, J., Sun, Y., Si, M., Liu, M., Li, J., Zhang, X., Shang, G., Tang, B., Yan, G., Zhou, C. Satellite Remote Sensing of Global Land Surface Temperature: Definition, Methods, Products, and Applications. Reviews of Geophysics. 2023, 61(1). https://doi.org/10.1029/2022rg000777

[2] Lin, L., Di, L., Zhang, C., Guo, L. The Global Land Surface Temperature Change in the 21st Century — A Satellite Remote Sensing Based Assessment. IEEE Journal of Selected Topics in Applied Earth Observations and Remote Sensing. 2024, 17, 1756–1764. https://doi.org/10.1109/jstars.2023.3338980

[3] Yu, Y., Privette, J. P., Liu, Y., Sun, D. Land Surface Temperature: Remote Sensing. 2020, pp. 33–38. https://doi.org/10.1201/9780429445552-6

[4] Keune, J., Schumacher, D. L., Dirmeyer, P., Miralles, D. G. Drought self-propagation in drylands through moisture recycling. EGU General Assembly 2022, Vienna, Austria, 2022. https://doi.org/10.5194/egusphere-egu22-9139

[5] Kroll, J., Stephan, R., Feldman, A. F., Miralles, D. G., Orth, R. Increased heating of the land surface as hot-dry events persist. EGUsphere [preprint]. 2025. https://doi.org/10.5194/egusphere-2025-4391

[6] Yoon, D., Chen, J.-H., Hsu, H., Findell, K. Different Roles of Land-atmosphere Coupling in Compound Drought-heatwave Events. EGU General Assembly 2025, Vienna, Austria, 2025. https://doi.org/10.5194/egusphere-egu25-1648

[7] Mangan, M. R. Evapotranspiration: Atmospheric boundary layer interactions across scales of surface heterogeneity. PhD thesis, Wageningen University, Wageningen, the Netherlands, 2025. https://doi.org/10.18174/681318

[8] Tabari, H. Contrasting responses of drought and floods to background aridity in a changing climate across global terrestrial ecosystems. EGU General Assembly 2024, Vienna, Austria, 2024. https://doi.org/10.5194/egusphere-egu24-8460

[9] Xiang, T., Vivoni, E. R., Gochis, D. J. Seasonal evolution of ecohydrological controls on land surface temperature over complex terrain. Water Resources Research. 2014, 50(5), 3852–3874. https://doi.org/10.1002/2013wr014787

[10] Guillod, B. P., Orlowsky, B., Miralles, D., Teuling, A. J., Blanken, P. D., Buchmann, N., Ciais, P., Ek, M., Findell, K. L., Gentine, P., Lintner, B. R., Scott, R. L., Van den Hurk, B., Seneviratne, S. I. Land-surface controls on afternoon precipitation diagnosed from observational data: uncertainties and confounding factors. Atmospheric Chemistry and Physics. 2014, 14, 8343–8367. https://doi.org/10.5194/acp-14-8343-2014

[11] McColl, K. A., He, Q., Lu, H., Entekhabi, D. Short-Term and Long-Term Surface Soil Moisture Memory Time Scales Are Spatially Anticorrelated at Global Scales. Journal of Hydrometeorology. 2019, 20(6), 1165–1182. https://doi.org/10.1175/jhm-d-18-0141.1

[12] Akter, T., Gazi, M. Y., Mia, M. B. Assessment of land cover dynamics, land surface temperature, and heat island growth in northwestern Bangladesh using satellite imagery. Environmental Processes. 2021, 8, 661–690. https://doi.org/10.1007/s40710-020-00491-y

[13] Brunsell, N. A. Characterization of land-surface precipitation feedback regimes with remote sensing. Remote Sensing of Environment. 2006, 100(2), 200–211. https://doi.org/10.1016/j.rse.2005.10.025

[14] Wan, Z., Hook, S., Hulley, G. MODIS/Terra Land Surface Temperature/Emissivity 8-Day L3 Global 1 km SIN Grid V061 [Dataset]. NASA EOSDIS Land Processes Distributed Active Archive Center, 2021. https://doi.org/10.5067/MODIS/MOD11A2.061

[15] Huete, A., Didan, K., Miura, T., Rodriguez, E. P., Gao, X., Ferreira, L. G. Overview of the radiometric and biophysical performance of the MODIS vegetation indices. Remote Sensing of Environment. 2002, 83(1–2), 195–213. https://doi.org/10.1016/S0034-4257(02)00096-2

[16] Weng, Q., Lu, D., Schubring, J. Estimation of land surface temperature–vegetation abundance relationship for urban heat island studies. Remote Sensing of Environment. 2004, 89(4), 467–483. https://doi.org/10.1016/j.rse.2003.11.005

[17] Tahasin, A., Haydar, M., Hossen, Md. S., Sadia, H. Drought vulnerability assessment and its severe impact on crop production and livelihood of people: An empirical analysis of Barind Tract. Research Square [preprint]. 2023. https://doi.org/10.21203/rs.3.rs-3378881/v1

[18] Wang, H., Xie, Q., Thompson, S. E., Moore, C. E., McGrath, G. S., Ruthrof, K. X. Subsurface constraints amplify vegetation stress during extreme heat and drought in a Mediterranean forest. Environmental Research Letters. 2025, 20(12), 124029. https://doi.org/10.1088/1748-9326/ae1e15

[19] Sarker, T., Reza, S., Roy, R., Uddim, T., Alif, S. A., Tariq, A. Geospatial mapping of heatwaves and drought: Exploring their link to vegetation, soil moisture, and groundwater in the thirsty Barind Tract, Bangladesh. Environmental Earth Sciences. 2026, 85(3), 88. https://doi.org/10.1007/s12665-025-12787-z

[20] Alizadeh, O. Changes in the mean and variability of temperature and precipitation over global land areas. Environmental Research: Climate. 2023, 2(3), 035006. https://doi.org/10.1088/2752-5295/ace279

[21] Bandari, A. Global precipitation varies with sea-surface temperature at different timescales. Scilight. 2019, 2019(25), 250012. https://doi.org/10.1063/1.5115011

[22] Simon, J. M., Ángel, G. M., Bradfield, L., Madeleine, C. T. Climate Variability and Trends. 2018, pp. 89–124. https://doi.org/10.4324/9781315115603-5

[23] Itzhak-Ben-Shalom, H., Alpert, P., Potchter, O., Samuels, R. MODIS Summer SUHI Cross-sections Anomalies over the Megacities of the Monsoon Asia Region and Global Trends. The Open Atmospheric Science Journal. 2017, 11(1), 121–136. https://doi.org/10.2174/1874282301711010121

[24] Munawar, M., McNeil, R., Jani, R., Buya, S., Tarmizi, T. Variations in land surface temperature increase in South-East Asian Cities. Environmental Monitoring and Assessment. 2025, 197(2), 190. https://doi.org/10.1007/s10661-024-13604-z

[25] Shawky, M., Ahmed, M. R., Ghaderpour, E., Gupta, A., Achari, G., Dewan, A., Hassan, Q. K. Remote sensing-derived land surface temperature trends over South Asia. Ecological Informatics. 2023, 74, 101969. https://doi.org/10.1016/j.ecoinf.2022.101969

[26] Dastour, H., Alam, M. M., Dewan, A., Hassan, Q. K. Evaluating climatic warming and the modulating effects of surface water and regional variables in western Bangladesh. Results in Engineering. 2025, 25, 103864. https://doi.org/10.1016/j.rineng.2024.103864

[27] Rakib, Z. Characterization of climate change in southwestern Bangladesh: trend analyses of temperature, humidity, heat index, and rainfall. Climate Research. 2018, 76(3), 241–252. https://doi.org/10.3354/cr01535

[28] Suhan, M. S. I., Adhikary, S. K. Exploring Climate Change Trends in Temperature and Rainfall Across the Southeastern Coastal Area of Bangladesh. Journal of Engineering Science. 2025, 15(2), 51–67. https://doi.org/10.3329/jes.v15i2.82162

[29] Haque, M. R., Arman, Moniruzzaman, M., Roy, S. K., Islam, A. K. M. S. Spatiotemporal trends and urban-climate interactions of land surface temperature dynamics across Bangladesh. Anthropocene. 2026, 54, 100547. https://doi.org/10.1016/j.ancene.2026.100547

[30] Liu, Y., Huang, Y., Yuan, J., Xie, Y., Zhou, C. Contribution of Surface Radiative Effects, Heat Fluxes and Their Interactions to Land Surface Temperature Variability. Journal of Geophysical Research: Atmospheres. 2024, 129(8). https://doi.org/10.1029/2023jd039495

[31] Brammer, H. Bangladesh's diverse and complex physical geography: implications for agricultural development. International Journal of Environmental Studies. 2016, 74(1), 1–27. https://doi.org/10.1080/00207233.2016.1236647

[32] Rashid, M. A., Ando, K., Tanaka, K., Kaida, Y. Village-Level Studies on Rice-Based Cropping Systems in the Low-Lying Areas of Bangladesh. II. Toposequence, hydrology, land classification and cropping patterns in the Bogra District of the Barind Tract. Japanese Journal of Crop Science. 1997, 66(1), 118–128. https://doi.org/10.1626/jcs.66.118

[33] Gorelick, N., Hancher, M., Dixon, M., Ilyushchenko, S., Thau, D., Moore, R. Google Earth Engine: Planetary-scale geospatial analysis for everyone. Remote Sensing of Environment. 2017, 202, 18–27. https://doi.org/10.1016/j.rse.2017.06.031

[34] Didan, K. MODIS/Terra Vegetation Indices 16-Day L3 Global 1 km SIN Grid V061 [Dataset]. NASA EOSDIS Land Processes Distributed Active Archive Center, 2021. https://doi.org/10.5067/MODIS/MOD13A2.061

[35] Funk, C., Peterson, P., Landsfeld, M., Pedreros, D., Verdin, J., Shukla, S., Husak, G., Rowland, J., Harrison, L., Hoell, A., Michaelsen, J. The climate hazards infrared precipitation with stations — a new environmental record for monitoring extremes. Scientific Data. 2015, 2, 150066. https://doi.org/10.1038/sdata.2015.66

[36] Food and Agriculture Organization of the United Nations. Global Administrative Unit Layers (GAUL) 2015, level 2 [Dataset]. Earth Engine Data Catalog, 2015. Available from: https://developers.google.com/earth-engine/datasets/catalog/FAO_GAUL_2015_level2

[37] Nugraha, A. S. A., Kamal, M., Heru Murti, S., Widyatmanti, W. Accuracy assessment of land surface temperature retrievals from remote sensing imagery: pixel-based, single and multichannel methods. Geomatics, Natural Hazards and Risk. 2024, 15(1). https://doi.org/10.1080/19475705.2024.2324975

[38] Duan, S.-B., Li, Z.-L., Li, H., Göttsche, F.-M., Wu, H., Zhao, W., Leng, P., Zhang, X., Coll, C. Validation of Collection 6 MODIS land surface temperature product using in situ measurements. Remote Sensing of Environment. 2019, 225, 16–29. https://doi.org/10.1016/j.rse.2019.02.020

[39] Xu, S., Wang, D., Liang, S., Liu, Y., Jia, A. Assessing the Reliability of the MODIS LST Product to Detect Temporal Variability. IEEE Geoscience and Remote Sensing Letters. 2023, 20, 1–5. https://doi.org/10.1109/lgrs.2023.3312384

[40] Yan, J., Ni, L., Li, X., Cheng, Y., Wu, H. A framework for reconstructing 1 km all-weather hourly LST from MODIS data. International Journal of Remote Sensing. 2023, 44(24), 7654–7677. https://doi.org/10.1080/01431161.2023.2242591

[41] Sen, P. K. Estimates of the regression coefficient based on Kendall's tau. Journal of the American Statistical Association. 1968, 63(324), 1379–1389. https://doi.org/10.1080/01621459.1968.10480934

[42] Mann, H. B. Nonparametric tests against trend. Econometrica. 1945, 13(3), 245–259. https://doi.org/10.2307/1907187

[43] Benjamini, Y., Hochberg, Y. Controlling the false discovery rate: A practical and powerful approach to multiple testing. Journal of the Royal Statistical Society: Series B (Methodological). 1995, 57(1), 289–300. https://doi.org/10.1111/j.2517-6161.1995.tb02031.x

[44] Zscheischler, J., Martius, O., Westra, S., Bevacqua, E., Raymond, C., Horton, R. M., Van den Hurk, B., AghaKouchak, A., Jézéquel, A., Mahecha, M. D., Maraun, D., Ramos, A. M., Ridder, N. N., Thiery, W., Vignotto, E. A typology of compound weather and climate events. Nature Reviews Earth & Environment. 2020, 1(7), 333–347. https://doi.org/10.1038/s43017-020-0060-z

[45] Zscheischler, J., Westra, S., van den Hurk, B. J. J. M., Seneviratne, S. I., Ward, P. J., Pitman, A., AghaKouchak, A., Bresch, D. N., Leonard, M., Wahl, T., Zhang, X. Future climate risk from compound events. Nature Climate Change. 2018, 8, 469–477. https://doi.org/10.1038/s41558-018-0156-3

[46] Gao, Y., Guilloteau, C., Foufoula-Georgiou, E., Xu, C., Sun, X., Vrugt, J. A. Soil Moisture-Cloud-Precipitation Feedback in the Lower Atmosphere From Functional Decomposition of Satellite Observations. Geophysical Research Letters. 2024, 51(22), e2024GL110347. https://doi.org/10.1029/2024gl110347

[47] Miralles, D. G., Holmes, T. R. H., De Jeu, R. A. M., Gash, J. H., Meesters, A. G. C. A., Dolman, A. J. Global land-surface evaporation estimated from satellite-based observations. Hydrology and Earth System Sciences. 2011, 15, 453–469. https://doi.org/10.5194/hess-15-453-2011

[48] Seneviratne, S. I., Corti, T., Davin, E. L., Hirschi, M., Jaeger, E. B., Lehner, I., Orlowsky, B., Teuling, A. J. Investigating soil moisture–climate interactions in a changing climate: A review. Earth-Science Reviews. 2010, 99(3–4), 125–161. https://doi.org/10.1016/j.earscirev.2010.02.004

[49] Ma, J., Shen, H., Jiang, M., Lin, L., Meng, C., Zeng, C., Li, H., Wu, P. A mechanism-guided machine learning method for mapping gapless land surface temperature. Remote Sensing of Environment. 2024, 303, 114001. https://doi.org/10.1016/j.rse.2024.114001

[50] Wang, T., Shi, J., Ma, Y., Husi, L., Comyn-Platt, E., Ji, D., Zhao, T., Xiong, C. Recovering Land Surface Temperature Under Cloudy Skies Considering the Solar-Cloud-Satellite Geometry: Application to MODIS and Landsat-8 Data. Journal of Geophysical Research: Atmospheres. 2019, 124(6), 3401–3416. https://doi.org/10.1029/2018jd028976

[51] Jiang, K., Pan, Z., Pan, F., Teuling, A. J., Han, G., An, P., Chen, X., Wang, J., Song, Y., Cheng, L., Zhang, Z., Huang, N., Ma, S., Gao, R., Zhang, Z., Men, J., Lv, X., Dong, Z. Combined influence of soil moisture and atmospheric humidity on land surface temperature under different climatic background. iScience. 2023, 26(6), 106837. https://doi.org/10.1016/j.isci.2023.106837

[52] Faisal, A.-A., Kafy, A.-A., Al Rakib, A., Akter, K. S., Jahir, D. M. A., Sikdar, M. S., Ashrafi, T. J., Mallik, S., Rahman, M. M. Assessing and predicting land use/land cover, land surface temperature and urban thermal field variance index using Landsat imagery for Dhaka Metropolitan area. Environmental Challenges. 2021, 4, 100192. https://doi.org/10.1016/j.envc.2021.100192

[53] Islam, M. T., Shahriar, M. A. Assessing the Effect of Land Use and Land Cover Changes on Land Surface Temperature in Jessore District, Bangladesh using Remote Sensing Techniques. Research Square [preprint]. 2023. https://doi.org/10.21203/rs.3.rs-3492845/v1

[54] Marufuzzaman, M., Khanam, M. M., Hasan, M. K. Monitoring the Land Cover Change and Its Impact on the Land Surface Temperature of Rajshahi City, Bangladesh using GIS and Remote Sensing Techniques. Journal of Geography, Environment and Earth Science International. 2021, 1–19. https://doi.org/10.9734/jgeesi/2021/v25i430278

[55] Ali, Y., Miah, M. D. Temporal and Spatial Variations in Surface Water and Its Interrelations with Land Surface Temperature and Rainfall Patterns in Chattogram City, Bangladesh. The Chittagong University Journal of Science. 2025, 45(1), 54–74. https://doi.org/10.3329/cujs.v45i1.79101

[56] Dewan, A., Kiselev, G., Botje, D., Mahmud, G. I., Bhuian, M. H., Hassan, Q. K. Surface urban heat island intensity in five major cities of Bangladesh: Patterns, drivers and trends. Sustainable Cities and Society. 2021, 71, 102926. https://doi.org/10.1016/j.scs.2021.102926

[57] Hossain, R. B., Ahmed, R., Sharmin, T., Refat, A., Moni, U. H. Spatiotemporal Analysis of Urban Expansion and Its Impact on Agricultural Land Degradation and Vegetation Health in Narayanganj District, Bangladesh. Acadlore Transactions on Geosciences. 2024, 3(4), 197–209. https://doi.org/10.56578/atg030402

[58] Goswami, M. M., Mujumdar, M., Singh, B. B., Ingale, M., Ganeshi, N., Ranalkar, M., Franz, T. E., Srivastav, P., Niyogi, D., Krishnan, R., Patil, S. N. Understanding the soil water dynamics during excess and deficit rainfall conditions over the core monsoon zone of India. Environmental Research Letters. 2023, 18(11), 114011. https://doi.org/10.1088/1748-9326/acffdf

[59] Taylor, C. M., Klein, C., Harris, B. L. Multiday Soil Moisture Persistence and Atmospheric Predictability Resulting From Sahelian Mesoscale Convective Systems. Geophysical Research Letters. 2024, 51(20). https://doi.org/10.1029/2024gl109709

[60] Meng, Q., Chen, S., Zhang, L., Zhu, X., Zhang, Y., Atkinson, P. M. GLOSTFM: A global spatiotemporal fusion model integrating multi-source satellite observations to enhance land surface temperature resolution. Remote Sensing of Environment. 2025, 319, 114640. https://doi.org/10.1016/j.rse.2025.114640

[61] Zarakas, C. M., Swann, A. L. S., Battisti, D. S. Land-Atmosphere Feedbacks Dampen Surface Evapotranspiration Fluxes in Wet Regions. ESS Open Archive [preprint]. 2024. https://doi.org/10.22541/essoar.173386151.15960422/v1

[62] Khanna, J., Cook, K. H., Vizy, E. K. Opposite spatial variability of climate change-induced surface temperature trends due to soil and atmospheric moisture in tropical/subtropical dry and wet land regions. International Journal of Climatology. 2020, 40(14), 5887–5905. https://doi.org/10.1002/joc.6554

[63] Pal, P., Bhattacharya, P. Soil physical properties: A crucial component of ecosystem health and productivity. International Journal of Agriculture and Nutrition. 2024, 6(2), 75–77. https://doi.org/10.33545/26646064.2024.v6.i2b.183

Biography

Nafia Muntakim is affiliated with the Institute of Environmental Science, University of Rajshahi, Bangladesh. Her research focuses on climate change and adaptation, heatwave vulnerability, urban resilience, human–environment interactions, water quality assessment, GIS, and remote sensing. She applies geospatial analysis, satellite remote sensing, statistical methods, and machine-learning approaches to investigate environmental and climatic problems. In the present study, she was responsible for conceptualization, methodology, formal analysis, and writing the original draft. Her broader research experience includes industrial effluent pollution, particulate air pollution, climatic drivers of lightning casualties, land-cover dynamics, surface urban heat islands, and compound hydroclimatic extremes. Her research interests particularly emphasize the application of geospatial and Earth observation data to environmental assessment and climate-resilient planning in Bangladesh.

Md. Imran Hossain is affiliated with the Institute of Environmental Science, University of Rajshahi, Bangladesh. His work applies geographic information systems and satellite remote sensing to environmental problems, with a particular focus on cloud-based geospatial processing in Google Earth Engine, multi-sensor image analysis, and the design of cartographic and statistical graphics for scientific publication. In the present study, he was responsible for validation, software implementation, and visualization, including the Earth Engine processing workflow and the preparation of the figures. His broader interests include spatial data quality assessment for long-term satellite records and the use of open Earth observation archives to support land and water management in Bangladesh.

Zihad Ahmed is an Assistant Professor in the Department of Geography and Environmental Studies, University of Rajshahi, Bangladesh. His research focuses on disaster management, environmental pollution and management, regional development planning, and human–environment interactions. His work applies geographical, geospatial, and community-based approaches to investigate environmental hazards, vulnerability, risk, and adaptation. In the present study, he was responsible for methodology and formal analysis. His broader research experience encompasses floods, riverbank erosion, cyclone vulnerability, earthquake hazards and preparedness, particulate air pollution, and environmental resource management. His research interests particularly emphasize understanding the spatial and socioeconomic dimensions of environmental hazards and supporting evidence-based disaster risk reduction, environmental management, and resilient regional planning in Bangladesh.

Md. Mizanoor Rahman is a Professor in the Department of Geography and Environmental Studies, University of Rajshahi, Bangladesh. His research focuses on environmental geography, climate adaptation planning, land and water resource management, rural livelihoods, drought, and regional development. His work examines the relationships among climatic hazards, environmental change, resource use, socioeconomic vulnerability, and livelihood adaptation, particularly in the context of Bangladesh. In the present study, he was responsible for supervision and for writing, reviewing, and editing. His broader research experience encompasses drought and its socio-economic impacts, cyclone vulnerability and adaptation, land-use transformation, rural and regional development, and sustainable resource management. His research emphasizes translating geographical and environmental evidence into effective strategies for climate adaptation, resource management, and regional development for vulnerable communities in Bangladesh.

Research Field

Nafia Muntakim: climate change and adaptation, heatwave vulnerability and urban resilience, GIS and remote sensing, hydroclimatic extremes, environmental pollution and water quality, human–environment interactions, geospatial statistical modelling

Md. Imran Hossain: geographic information systems, Google Earth Engine analysis, geospatial data visualisation, remote sensing image processing, spatial data quality assessment, cartography

Zihad Ahmed: disaster management, environmental pollution and management, regional development planning, climate-related hazards, human–environment interactions, and geospatial assessment of environmental risk

Md. Mizanoor Rahman: climate change and adaptation planning, environmental pollution, environmental disasters, vulnerability and adaptation, economic transformation, and regional planning